Connection between the physicochemical characteristics of amorphous carbon thin films and their electrochemical properties

Elli Leppänen[1], Anja Aarva[1], Sami Sainio[2,3], Miguel A. Caro[1] and Tomi Laurila[1,4]

[1] Department of Electrical Engineering and Automation, School of Electrical Engineering, Aalto University, Tietotie 3, 02150 Espoo, Finland

[2] Stanford Synchrotron Radiation Lightsource, SLAC National Accelerator Laboratory, Menlo Park, CA, 94025, USA

[3] Microelectronics Research Unit, Faculty of Information Technology and Electrical Engineering, University of Oulu, P.O. Box. 4500, 90570 Oulu, Finland

[4] Department of Chemistry and Materials Science, Aalto University, Kemistintie 1, 02150 Espoo, Finland

Abstract

Connecting a material's surface chemistry with its electrocatalytic performance is one of the major questions in analytical electrochemistry. This is especially important in many sensor applications where analytes from complex media need to be measured. Unfortunately, today this connection is still largely missing except perhaps for the most simple ideal model systems. Here we present an approach that can be used to obtain insights about this missing connection and apply it to the case of carbon nanomaterials. In this paper we show that by combining advanced computational techniques augmented by machine learning methods with x-ray absorption spectroscopy (XAS) and electrochemical measurements, it is possible to obtain a deeper understanding of the correlation between local surface chemistry and electrochemical performance. As a test case we show how by computationally assessing the growth of amorphous carbon (a-C) thin films at the atomic level, we can create computational structural motifs that may in turn be used to deconvolute the XAS data from the real samples resulting in local chemical information. Then, by carrying out electrochemical measurements on the same samples from which x-ray spectra were measured and that were further characterized computationally, it is possible to gain insight into the interplay between the local surface chemistry and electrochemical performance. To demonstrate this methodology, we proceed as follows: after assessing the basic electrochemical properties of a-C films, we investigate the effect of short HNO_3 treatment on the sensitivity of these electrodes towards an inner sphere redox probe (ISR) dopamine (DA) to gain knowledge about the influence of altered surface chemistry to observed electrochemical performance. These results pave the way towards a more general assessment of electrocatalysis in different systems and provide the first steps towards data driven tailoring of electrode surfaces to gain optimal performance in a given application.

Keywords: electrocatalysis, amorphous carbon, x-ray spectroscopy, density functional theory, machine learning

Introduction

Amorphous carbon (a-C) and, especially, its high sp^3 bonded carbon form, known as tetrahedral amorphous carbon (ta-C), is a promising electrode material owing to its several unique electrochemical properties, such as chemical inertness and resulting wide potential window as well as low background current. Thus, ta-C has been used in many electroanalytical applications ranging from detection of biomolecules [1–4] to trace analysis of heavy metals [5]. The basic electrochemical properties and response of ta-C to several redox systems have also

been investigated [6–9] and recently reviewed [10]. The unique electrochemical properties of ta-C originate from the specific structural features of the material in thin film form, as recently discussed in [11]. One of the main factors that determine the properties of a given a-C material is the ratio of sp^3 to sp^2 bonded carbon in the film. In this paper, we will thoroughly discuss the physical origin of these special structural features, which can be traced back to the growth conditions, as highlighted in our recent computational work [12,13] on how ta-C (as well as a-C) films are formed at the atomic level. The electrochemical properties of these thin film materials are strongly influenced by their surface chemistry. We will present our recent scheme to deconvolute experimental x-ray spectroscopy spectra to gain atomic level information about the chemistry of a-C surfaces. This data will be used to create computational structural models based on real sample information, in contrast to the highly idealized models commonly employed in the literature, that fail to capture the chemical and structural richness of a-C materials [14,15]. We will not go into the details of the relationship between the structural and electrical properties of ta-C thin film electrodes, which have been summarized by us elsewhere [16]. We will then proceed to investigate the effect of the frequently utilized short HNO_3 treatment on the surface chemistry of ta-C thin films. Finally, we will study how the chemical and structural changes in the films, induced by the nitric acid treatment, are reflected in the electrochemical behaviour of these thin film electrodes. At all stages of discussion, we will try to utilize a tight combination of experimental and computational studies to obtain a more comprehensive understanding of the observed results.

Methodology

The deposition process for the ta-C films has been described in detail in [11] and is thus only briefly described here. ta-C samples (about 7 nm thick films) were deposited at room temperature on boron doped p-type silicon (100) prime wafers (<0.005 Ωcm, Siegert Wafer), with 20 nm thick Ti adhesion layer with a pulsed filtered cathodic vacuum arc system (p-FCVA) in a vacuum chamber evacuated to base pressures below 5×10^{-7} Torr using a CTI cryogenics CTI 8F cryopump.

The p-FCVA system uses a toroidal 45° bent electromagnetic filter, with a pulse forming network unit of 2.6 mF charged to - 400 V (pulse current 650 A, 1 Hz). The source material for the carbon plasma is a graphite rod of 6.35 mm diameter and purity of 99.95 % (Graphitestore).

The amorphous carbon films were deposited on highly conductive, boron-doped (100) Si wafers (Ultrasil) with closed-field unbalanced magnetron sputtering operated in DC mode. The target was a 4-inch graphite disk (99.99 % purity). The DC power was varied between 800 and 2000 W corresponding to power densities of 10 and 25 W/cm^2, respectively. The working pressure was 3 mTorr and the argon flow was kept constant at 80 sccm during deposition with a mass flow controller. The substrates were mounted on a rotating sample holder and rotated at 20 rpm during deposition. The deposition rates were calculated with an Alpha-Step IQ profilometer (KLA-Tencor) and deposition times were adjusted to obtain 100 nm thick films.

Here three types of samples were investigated: i) untreated a-C, ii) untreated ta-C and iii) HNO_3 treated ta-C, where 70 % HNO_3 was drop-casted on top of the sample. After a 5 minute wait, the sample was washed three times in deionized water.

Experimental XAS spectra were collected at beamline 8-2 at the Stanford Synchrotron Radiation Lightsource (SSRL). Experimental details are described in detail in our previous work [17].

Computational fitting of XAS spectra is based on a method introduced in [1, 2]. It relies on reference spectra that are computed at the density functional theory (DFT) level, from a large computational dataset of atomic structural models. The spectra are then grouped together by unsupervised machine learning (ML) clustering technique in order to reduce complexity, and averaged. Finally, these "fingerprint spectra" are used to fit experimental spectra by creating the best matching spectra that can be constructed from a linear combination of fingerprint spectra.

Cyclic voltammetry (CV) was carried out with a Gamry Reference 600+ potentiostat, where a three-electrode cell was used for all measurements with an Ag/AgCl

(+0.199 V vs. SHE, Radiometer Analytical) reference electrode and a Pt wire (Goodfellow) as a counter electrode. Electrochemical measurements were carried out with untreated ta-C and HNO_3 treated ta-C. The measurements were conducted in 1 mM $Ru(NH_3)_6^{2+/3+}$, 1 mM $IrCl^{3-/2-}$ and 100 μM dopamine (DA), where hexaamineruthenium(III) chloride (Sigma-Aldrich) and potassium hexachloroiridate(IV) (Aldrich) were dissolved in 1 M KCl (Merck Suprapur, pH 6.8), whereas dopamine hydrochloride (Sigma-Aldrich) was dissolved in 10 mM phosphate-buffered saline (PBS, pH 7.4). In addition, potential windows for both samples were measured in 0.1 M $HClO_4$ (VWR Chemicals, pH 1). All solutions were purged with N_2 for 30 min prior to the measurements. Furthermore, all experiments were conducted at room temperature in a Faraday's cage, where a new electrode was prepared for every electrochemical measurement.

Formation of a-C films

The growth of a-C films takes place via deposition of energetic atoms onto a substrate, e.g., by cathodic arc deposition, or following other physical or chemical deposition techniques [10]. Obtaining insight into the growth mechanism experimentally is extremely challenging, and the nature of deposition-mediated growth has made reproducing it via accurate computer simulation impractical until recently. Therefore, the underlying physical processes leading to the formation of a-C and, in particular, the high-density "diamond-like" form, ta-C, have remained poorly understood until machine learning (ML) potentials provided an acceptable tradeoff between accuracy and computational cost [12,13]. Using a Gaussian approximation potential (GAP [18], a specific flavor of ML interatomic potentials) for a-C [19], we recently managed to carry out large-scale deposition simulations to mimic the experimental conditions under which a-C grows during cathodic arc deposition, from low to high energy or, equivalently, from low to high density. The details of the calculations and our methodology can be found in [13]; here we just briefly summarize the results. Figure 1 shows the evolution of the a-C structure as a function of deposition energy, which is positively correlated with the sp^3 fraction and mass density, assuming that the films contain only low amounts of elements other than carbon (for example, H can increase sp^3 content in a-C:H by saturating the carbon bonds, without increasing mass density). As the deposition energy decreases, the fraction of sp^3 bonded carbon decreases accordingly, and the structure becomes less dense and graphitic like. The surface roughness increases both for low energy deposition and very high energy deposition; the smoothest a-C films are predicted at deposition energies from 5 eV to 20 eV, approximately. It was also shown in [13] that low density films contained a notable amount
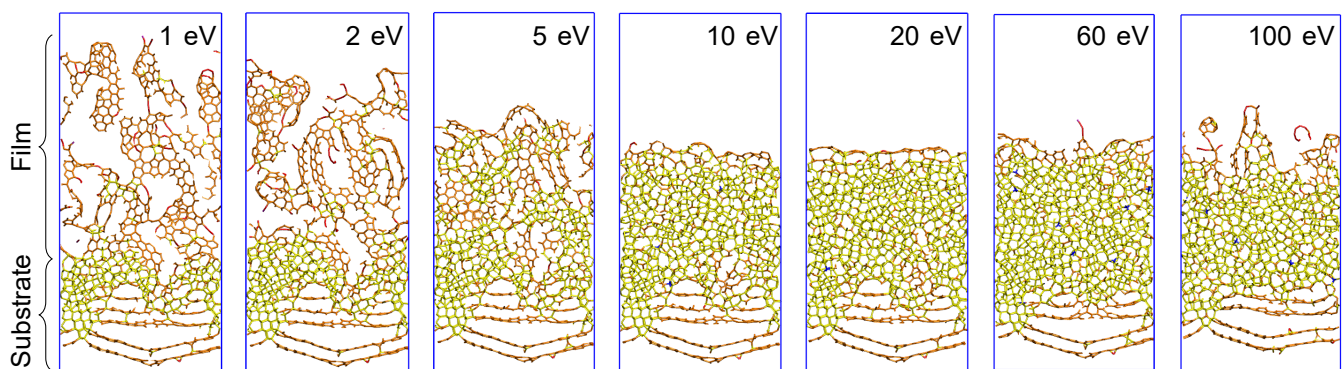

Figure 1. The nanostructure of deposited a-C films changes as a function of deposition energy, from low-density graphitic carbon at low deposition energy to dense diamond-like carbon at high deposition energy. Here we show two-dimensional slices through the simulated films, to highlight the local structural environments: predominantly sp^2 (orange) at low density and predominantly sp^3 (yellow) at high density. Coordination defects, namely sp chains and 5-fold sites, are colored in red and blue, respectively. Reprinted figure with permission from Caro et al., Phys. Rev. B 102, 174201 (2020). Copyright (2020) by the American Physical Society.

of highly reactive sp bonded carbon, the fraction of which decreases rapidly as the density (deposition energy) increases. Under atmospheric conditions these sites are, however, rapidly passivated, a result which is supported also by the simulation work [20]. Furthermore, it was observed that the films deposited in the range of 5 eV exhibited clearly distinct regions of diamond likeness (high sp^3) or graphite likeness (high sp^2), making the film structure patch-like, which may have implications for the electrical properties of the resulting films. As is evident from the figure, the growth mechanism of a-C is strongly dependent on the impacting atom's energy (as is the resulting structure). At high energies, our simulations suggest "peening" to be the dominant mechanism and formation of ta-C type of structure [12], whereas, at low energies, the simulated films grow predominantly by direct formation of sp^2 motifs around the impact site, resulting mainly in a-C formation. These two growth mechanisms are schematically depicted in Figure 2. A notable additional feature in a-C films, even at high density, is the presence of an sp^2 rich layer at the film's surface (Figure 1). This implies not only that the surfaces are chemically rather similar, but also that the electron transfer at the surfaces of a-C electrodes should be more or less independent of the sp^3 fraction in the bulk of the films. In fact, as was shown in [11], with outer sphere probes (OSR) the reaction kinetics on ta-C electrodes with different
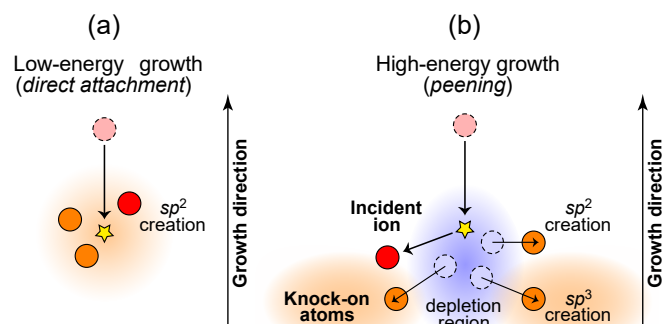

Figure 2. The growth mechanism of a-C as inferred from deposition simulations is "direct attachment" at low deposition energies and "peening" at high deposition energies. The peening mechanism involved local destruction of sp3 carbon at the site of impact, but an overall increase in sp3 fraction due to built-up lateral pressure. Reprinted from Caro et al., Phys. Rev. B **102**, 174201 (2020). Copyright (2020) by the American Physical Society.
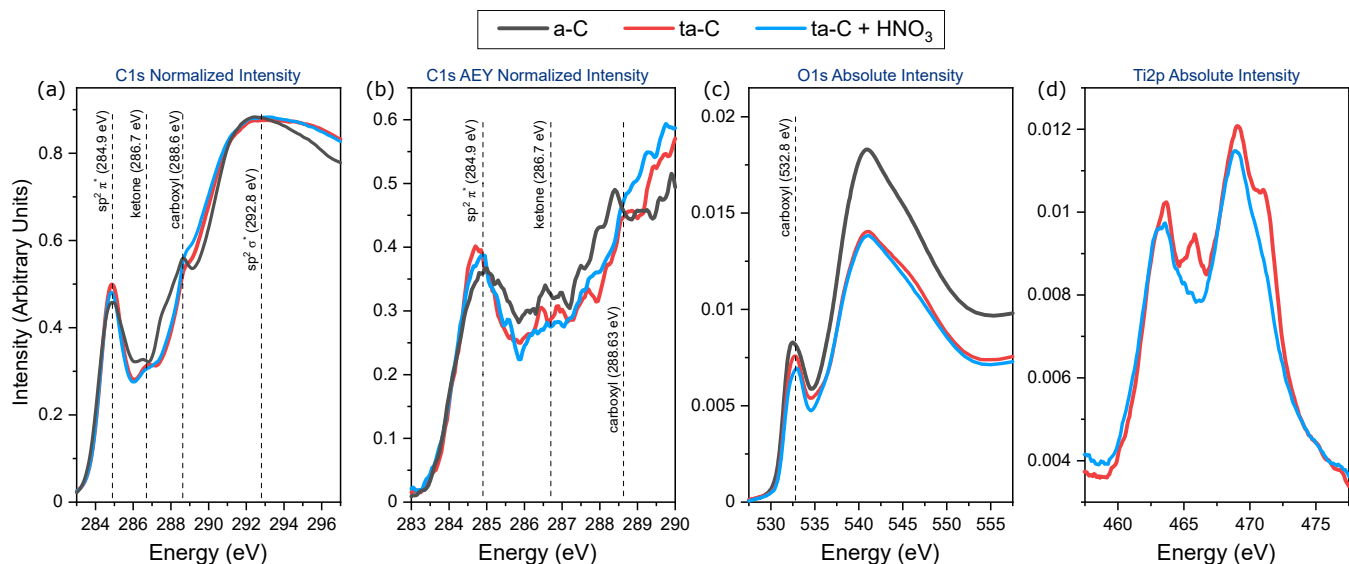
thicknesses is controlled by the electron transport through the films, rather than the electron transfer at the surface. The situation becomes entirely different when surface sensitive inner sphere redox (ISR) probes are utilized. The thickness of the surface layer is also deposition energy dependent, being thicker (and rougher) at high energies. Since the sp^2 rich surface layer is expected to be rather reactive [20,21], this feature enables tailoring of the surface chemistry for specific purposes. To gain insight into the surface chemistry of a-C films, one needs a detailed description of local chemical and structural information, and to build a connection between the simulated structures and experimental observables. Hence, the structural models presented here were utilized in the deconvolution of x-ray absorption spectroscopy (XAS) data to match the experimental information with the local atomic level properties and provide us with realistic model surfaces based on real samples.

Local surface chemistry

In order to gain insight into the surface chemistry of the carbon films, XAS analyses were carried out followed by the computational deconvolution of the spectra. We will start by analyzing the experimental spectra, first the overall trends seen with all the three carbon materials and then the differences between reference ta-C and HNO$_3$ treated ta-C films in more detail. This is because the latter results will be subsequently connected with the observed electrochemical performance of these two types of samples. XAS total electron yield (TEY) spectra (shown in Figure 3) reveal that the main differences between a-C, ta-C and ta-C + HNO$_3$ samples are (*i*) in their overall oxygen content, (*ii*) carbon to oxygen ratio, (*iii*) amount and nature of oxygen containing functional groups as well as (*iv*) in the sp^2 π^* intensity and peak width (the differences in the peak width are attributed here mainly to non-carbon compounds bonded in the carbon network, as all of the films studied here are amorphous). In the normalized C1s spectra (Figure 3a), the a-C samples have slightly higher π^* characteristics than the ta-C in the region after the sp^2 π^* main peak at 284.9 eV up until after the carboxyl peak at 288.6 eV (indicating overall higher carbon-oxygen bonding in the a-C samples). Also, the ta-C + HNO$_3$ display lower sp^2

Figure 3. XAS C1s, O1s and Ti2p spectra. In (a), (c) and (d) data was collected in the total electron yield mode whereas in (b) Auger electron yield mode.

π^* contribution than the untreated ta-C. Area between the energy range of 285 - 292 eV corresponds to carbon-oxygen and carbon-nitrogen bonds found in the material. The fact that this region is not flat indicates high amounts of non-carbon contaminants being bound to the carbon matrix. Based on the earlier studies, we expect the majority of this increased intensity to arise from oxygen loading [17]. Additionally, there is a clear and sharp feature around 288.7 eV indicating clear presence of carboxyl-like groups especially on the a-C, also seen as a clear shoulder in the ta-C + HNO$_3$ sample.

Moving on to the more detailed differences between ta-C and ta-C treated with HNO$_3$ the following observations can be made. As already noted above, based on the C1s spectra from TEY measurements (*i*) the ta-C film treated with HNO$_3$ shows a clear increase in carboxyl groups and (*ii*) an decrease in the sp^2 contribution (this may however mainly come from the "bulk" as the films are only 7 nm thick, which is close to the probing depth of TEY). On the other hand, the only marked change when looking at the immediate surface (as revealed by the Auger electron yield (AEY) spectrum in Figure 3b) is the increase in carboxyl groups and no differences in the sp^2 contribution can be seen between the two samples. The above noted changes are clear albeit not very large. While looking at the differences in the O1s spectra (shown in Figure 3c), it can be seen that

in the HNO$_3$ treated sample, the overall carboxyl (note that this means carboxyl in C, as there are also plenty of other groups that have peaks around the same energy that are not bound to carbon) intensity is decreased in the non-normalized O1s spectra. This is likely related to the fact that the surface chemistry changes with the acid treatment, causing the overall oxygen coverage on the surface to decrease most likely by removal of impurity species from the material surface. However, analysis of the C1s spectra actually reveals that the ratio of O to C and the amount of carboxylic acid both increase after the HNO$_3$ treatment. The N1s spectra, on the other hand (see Supporting Information), show very low intensity on both types of samples, and one cannot conclude that the HNO$_3$ treatment would bring N to the system. Ti2p spectrum in Figure 3d shows consistent results to the ones discussed above, as the overall intensity, like in the O1s spectrum, is also decreased after the treatment. It is likely that this decrease seen in O1s is related to the subtle changes observed in Ti2p spectrum. Unfortunately, the O1s AEY counts were too low for us to make any reasonable further analysis regarding bulk vs. surface regions. Thus, the main conclusions are that (*i*) there is an increase in the carboxylic acid functionalities on the HNO$_3$ treated surface as compared to the untreated one and (*ii*) the carbon-to-oxygen ratio changes on the surface of the films so that there is more oxygen relative to carbon in HNO$_3$ treated than in

untreated ta-C samples. This is evident even though the overall oxygen signal indicates that the total amount of oxygen in the sample is decreased. The latter may be related to HNO_3 treatment induced changes in the TiO_x adhesion layer and/or cleaning of the surface from the impurities, but further investigations are required to verify this.

Next we used our previously established computational deconvolution scheme based on the structural motifs gained from the growth simulations of a-C and ta-C to extract atomic level chemical information from the experimental spectra (see Figure 4 for schematic presentation). In this computational fitting scheme [14,15] we include the whole shape of the spectrum, i.e, a fingerprint that comes from a specifically bonded site to the experimental sample, instead of only peak positions from literature references. In this case, we are comparing three different types of samples: amorphous carbon (a-C) [22] and tetrahedral amorphous carbon (ta-C) [1] with or without nitrogen acid treatment [23]. From the computational fit we can clearly see (Figure 5) that the nitric acid treatment does not necessarily remove oxygen from the sample as was concluded in Ref. [24] and indicated by the experimental O1s spectra here. Further, the sp^2 contribution appears larger in the case of a-C ($\sim$ 4.2 %) and ta-C ($\sim$ 0.7 %) samples with nitric acid

treatment than without it, as was also observed in Ref. [28], but contrary to what was stated above. However, as was discussed above, the changes in the sp^2 contribution were seen only in the TEY spectrum and not in the AEY spectrum and therefore arise at least partly because of the bulk contributions, which are absent here. Similarly the overall loss in oxygen content observed in the experimental spectra can be related to removal of impurities and/or changes in the chemistry of TiO_x adhesion layer that are not included in this computational scheme. The trend related to the amount of carboxylic acid (COOH) in different samples follows that of previously reported in [3] and is also consistent with the present TEY and AEY results. As COOH is one of the most solid references to be noticed, both experimentally and computationally, it easily stands out [14,15]. Other groups, such as ketones, hydroxyls, ethers and epoxides, may thus be hidden because of the overlapping features especially in the experimental spectra; however, their presence should not be neglected, and their existence can in fact be computationally verified as shown by the present results.

These results, that can - in fact - be contradictory with the traditional interpretation, suggest that all samples have very similar amounts of ketones (=O) and hydroxyl groups (-OH). They are both overlapping features with
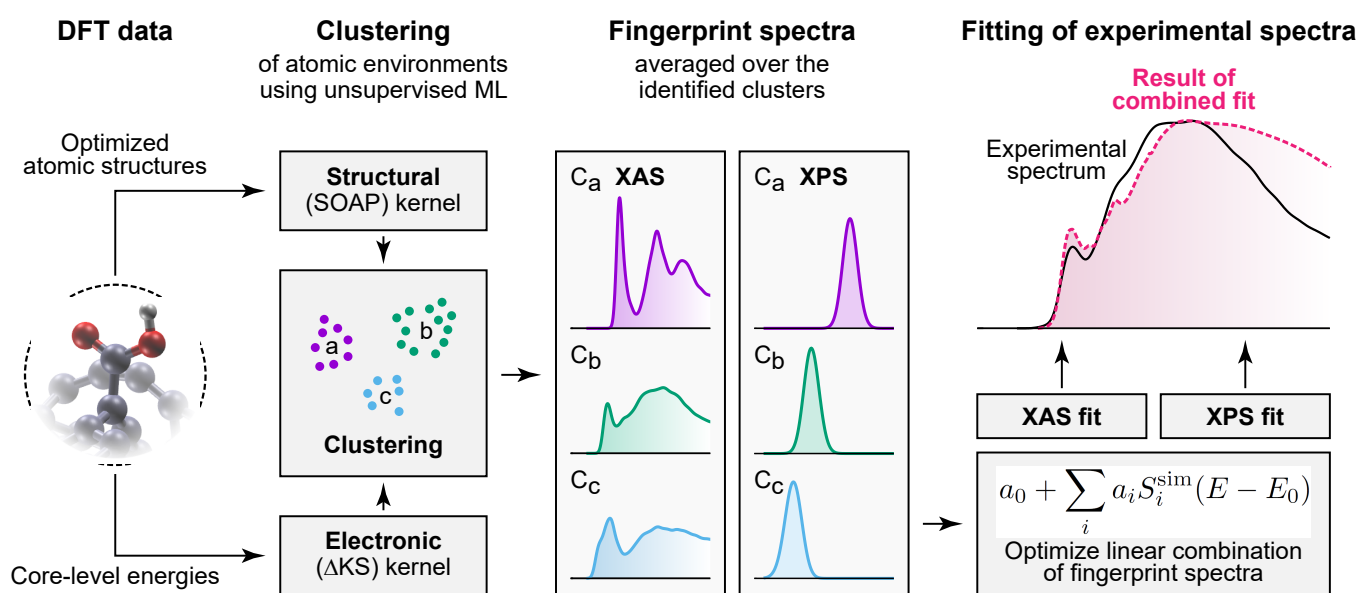

Figure 4. This approach [14,15] works in following way: (1) we have computational data from DFT calculations; (2) this data is clustered according to unsupervised machine learning [25–27] in order to obtain an average spectrum for each cluster; (4) and then we can compare the computational spectra with the real experiment. Reprinted figure with permission from Aarva et al., Chem. Matter. 31, 9256-9267, (2019). Copyright (2019) by the American Chemical Society. https:// pubs.acs.org/doi/abs/10.1021/acs.chemmater.9b02050.
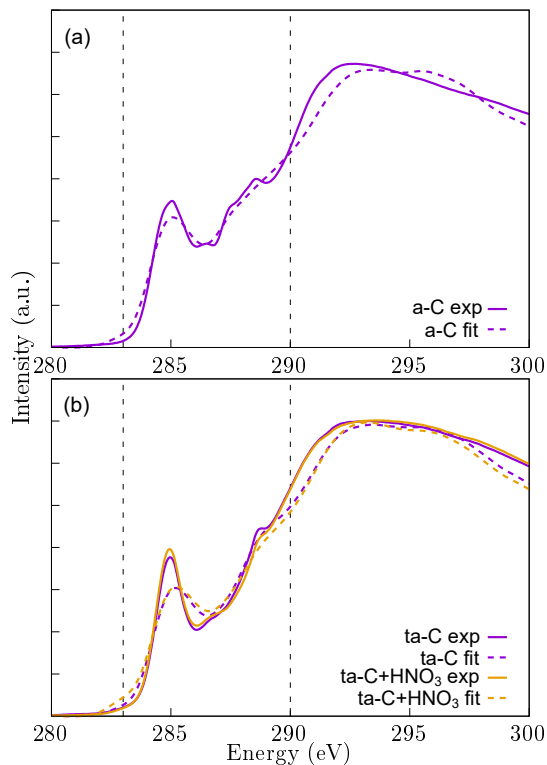
Figure 5. This is an example of computational fitting of some new experimental spectra, that are discussed more in the text. Interpretations about the results may vary according to the methodology used, but the similarities encourage us to employ these methods and read the results in more reliably than never before.

Figure 6: (a) Potential window in 0.1 M $HClO_4$ (v = 100 mV/s), (b) $Ru(NH_3)_6^{2+/3+}$ in 1 M KCl (v = 50 mV/s), (c) $IrCl_6^{3-/2-}$ in 1 M KCl (v = 50 mV/s) and 100 μM of DA in 10 mM PBS (v = 50 mV/s).

Table 1. The average values ($N = 3$) of potential windows and double layer pseudocapacitance C_{dl} at different potentials in 0.1 M $HClO_4$ at scan rate $v = 100$ mV/s.

Sample	Potential window (V)	C_{dl} (μF)		
		$E = -0.5$ V	$E = 0.25$ V	$E = 1.0$ V
ta-C	2.91 ± 0.12	8.9 ± 0.6	6.6 ± 0.6	6.7 ± 0.2
ta-C + HNO$_3$	2.88 ± 0.23	10.2 ± 0.3	5.6 ± 1.4	7.6 ± 2.1

respect to the clustering and visual interpretation [14, 15]. The numbers are between 0.6% to 0.7%, but they should not be taken as exact values. The method allows to have only semi-quantitative estimations. The nitric acid treated ta-C stands out with a higher amount of ethers and / or epoxides (~ 4%), from which epoxides are known to be more reactive [20,29]. Where as the a-C and ta-C samples have approximately same amount (~ 3%) of these functional groups. Unfortunately, in case of a-C, there are so many overlapping features, that it is not sound to read the results as verbatim. However, when experimental and computational results agree, we feel that the results are on solid ground.

As the finer nuances of the surface chemistry are out of the scope of the present manuscript, we do not go into the more detailed analysis of the computational spectra and only conclude that the experimental and computational results agree well on the main findings.

Electrochemistry

After acquiring detailed information about the changes in the surface chemistry of ta-C films after the HNO$_3$
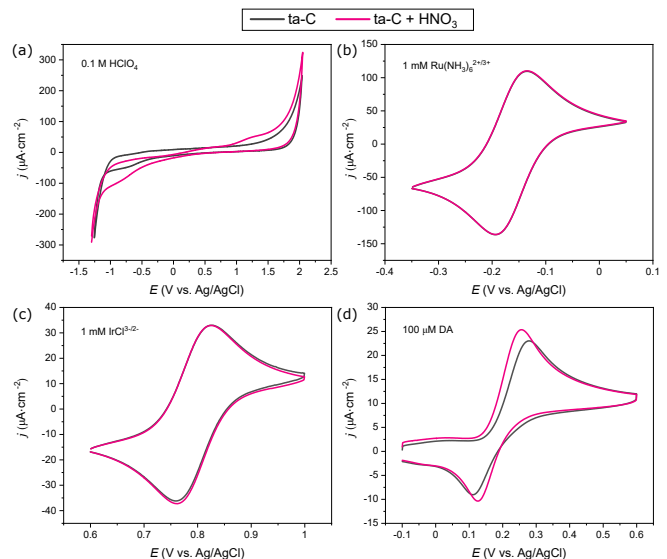
treatment we proceeded to investigate the subsequent effects on the electrochemical behavior. The blank voltammograms in $HClO_4$ for the both electrodes are shown in Figure 6a. The major features are quite similar, meaning that the background current and thus the double layer pseudocapacitance as well as the onset potentials for hydrogen evolution and oxygen evolution reactions (HER and OER) are about the same (see Table 1). A shoulder around 1.25 V (vs Ag/AgCl) is, however, seen in the case of HNO$_3$ treated ta-C electrode, indicating that some faradaic process that is not present in the untreated ta-C occurs at that potential range. The shoulder is in a voltage range where several oxygen and nitrogen based groups are known to oxidize (Figure 7). As the XAS results showed that there was practically no nitrogen in the films we can concentrate only in enols, methoxy and carboxylic acid groups. The experimental spectra cannot hep us in here as all oxygen group features other than those of carboxylic acid are highly convoluted. However, based on the computational fitting scheme we can rule out also enols and methoxies as they
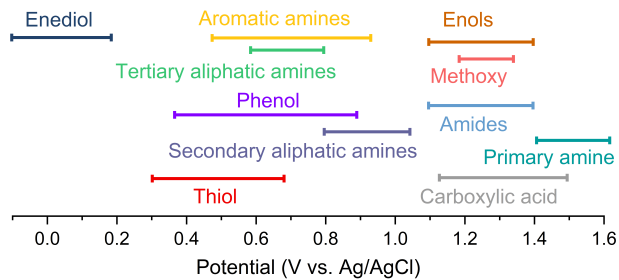
Figure 7: Approximate oxidation potentials of various functional groups on Pt and carbon electrodes [30].

do not appear as fingerprints in the computational scheme. Also at the cathodic end, the CV curve of the HNO_3 treated sample is slightly more suppressed indicating perhaps the stronger influence of residual oxygen in the cell to cathodic current. However, the overall shape appears to be the same in both cases.

The potential of zero total charge (pztc) of ta-C is around 0.27 V (vs. Ag/AgCl) in $HClO_4$ and it will shift towards 0 V as the pH increases towards neutral values [21]. Likewise, we know that the isoelectric point (IP) of plain ta-C is around pH 2.6, indicating that the surface functional groups are acidic. Based on the XAS and potential window measurements, we can expect that HNO_3 treatment increases the acidity a bit (more carboxylic groups on the surface), but most likely does not change the overall trends in pztc or IP. Thus, in order to see if there are (*i*) changes in the electronic properties of ta-C surface layer because of the HNO_3 treatment and (*ii*) possible electrostatic effects arising from the changes in the charge of the surface, we utilized two surface insensitive OSR probes [$Ru(NH_3)_6^{2+/3+}$ and $IrCl_6^{3-/2-}$] with not only of different charge, but also with widely different formal potentials [that of $Ru(NH_3)_6^{2+/3+}$ is about -0.16 V (vs. Ag/AgCl) and that of $IrCl_6^{3-/2-}$ is about +0.79 V (vs. Ag/AgCl)]. Thus, the two probes should see a

differently charged surface during their redox reactions. However, based on Figure 6b,c and Table 2 both probes showed nearly reversible electron transfer on both types of electrodes and no marked electrostatic effects were observed. In order to assess the degree of reversibility of the reactions more quantitatively, the values of the parameter Λ, proposed by Matsuda and Ayabe [31], were also calculated. The following limits of Λ are used to distinguish reversible, quasi-reversible and irreversible cases:

Reversible: $\Lambda \geq 15$ $k^0 \geq 0.3\ (n\upsilon)^{0.5}\ cm\ s^{-1}$

Quasi-reversible: $15 > \Lambda > 10^{-3}$ $0.3 \times 12 > k^0 > 2 \times 10^{-5}\ (n\upsilon)^{0.5}\ cm\ s^1$

Irreversible: $\Lambda \leq 10^{-3}$ $k^0 \leq 2 \times 10^{-5}\ (n\upsilon)^{0.5}\ cm\ s^{-1}$

Values of this parameter listed in Table 2 show that the ET reaction for the $IrCl_6^{3-/2-}$ was quasi-reversible whereas that of $Ru(NH_3)_6^{2+/3+}$ was practically reversible at all investigated scan rates (up to 1 V/s). Thus, the surface treatments had no significant effects on ET dynamics in either one of the electrodes indicating that electronic properties of the immediate surface region were not affected by the treatment. This is consistent with the results from the AEY and computational analyses showing practically no changes in the sp^2 contribution at the surface.

As there were no changes in ET rates induced by the surface treatments in the case of OSR probes, we turned next to the surface sensitive ISR probe dopamine (DA) to see whether the chemical changes after the treatment revealed by the XAS and computational results would affect its behaviour. Figure 6d shows the CV measurements of 100 µM of DA in PBS at 50 mV/s. As can be seen there is a slight cathodic shift in the

Table 2. Results of the cyclic voltammetry measurements in $Ru(NH_3)_6^{2+/3+}$, $IrCl^{2-/3-}$ and DA with scan rate $v = 50$ mV/s. k^0 is evaluated with Nicholson's method [32], whereas Λ with Matsuda and Ayabe [31]. For all measurements $N = 3$.

Sample	$Ru(NH_3)_6^{2+/3+\ (a)}$				$IrCl^{2-/3-\ (b)}$				DA			
	ΔE_p (mV)	$i_{p,a}/i_{p,c}$	$k^{0\ (b)}$ (cm·s^{-1})	$\Lambda^{(b)}$	ΔE_p (mV)	$i_{p,a}/i_{p,c}$	$k^{0\ (b)}$ (cm·s^{-1})	$\Lambda^{(b)}$	ΔE_p (mV)	$E_{p,a}$ (mV)	$E_{p,c}$ (mV)	$i_{p,a}/i_{p,c}$
ta-C	60 ± 1	0.92 ± 0.06	0.23 ± 0.13	42 ± 5	68 ± 4	0.98 ± 0.01	0.03 ± 0.01	9 ± 12	172 ± 6	280 ± 4	108 ± 8	1.4 ± 0.1
ta-C+ HNO_3	59 ± 0	0.91 ± 0.02	0.23 ± 0.12	42 ±5	64 ± 5	0.95 ± 0.01	0.05 ± 0.13	12 ± 14	136 ± 7	260 ±2	124 ± 3	1.3 ± 0.1

(a) Diffusion coefficients used in k^0 calculations taken from [33,34]

(b) The average value and standard deviation are calculated from several measurements at scan rates $v = 10, 50, 100, 200$ and 400 mV/s

oxidation peak potential (and subsequent decrease in peak separation) after the HNO₃ treatment. As there were no changes in the electronic structure of the surfaces or transport properties of the ta-C film, there are two likely origins of this behaviour. First one is related to the possibility of weak adsorption of the oxidized form of DA (DAQ), which would result in the decrease of the activation energy for the oxidation reaction and subsequent decrease in the required overpotential. The energetic view is shown in Figure 8, drawn at the formal potential of the reaction, where the adsorption stabilizes the product and shifts its Gibbs free energy curve (this is a schematic 2D section taken from a multidimensional plot) downward. If we assume that the interaction between DA and surface is not too strong (as must be the case because of the small shift in potential) to change the shape of the Gibbs energy curves near their crossing point, we obtain the situation shown in Figure 7. Thus, one can see that the activation energy of the oxidation reaction becomes smaller, which means that less overpotential is required to drive the reaction and thus there will be a cathodic shift in the oxidation peak potential. During the backward scan the activation should of course be slightly higher for the reduction, as the oxidized form (the reactant) is now effectively sitting at the bottom of the adsorption energy well. However we do not see any clear p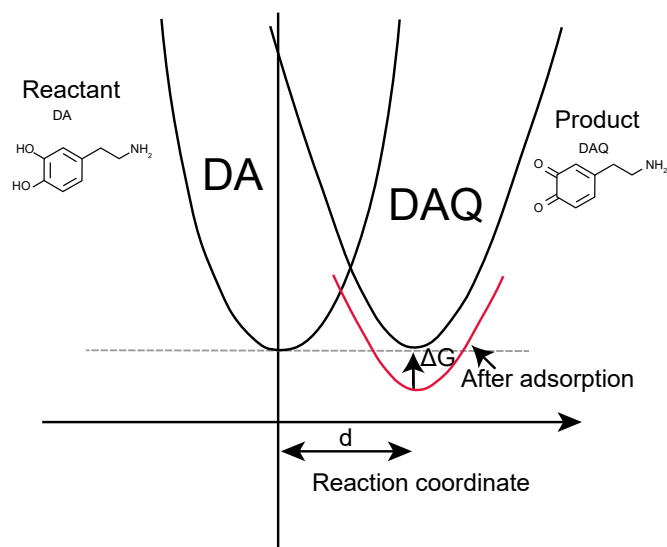otential shift here, which might be masked by the increasing cathodic current (see Table 2 and changes in $i_{p,a}/i_{p,c}$) in comparison to the untreated ta-C due to the presence of the weakly adsorbed oxidized form (DAQ) next to the electrode readily available for the reduction reaction. As seen in Fig. 6d ascending slopes of both the oxidation and the reduction peaks become steeper after the HNO₃ treatment of the ta-C and the change appears to be larger in the case of the reduction peak. In the latter case also the descending part of the peak is slightly steeper than that for a typical diffusion controlled reaction consistent with the assumption of the weak adsorption of the DAQ in this system. Further, our earlier computational results [35] indicate that the adsorption strength of DAQ increases as the surface of the ta-C electrode becomes negative (Figure 9).

As noted above, ptzc of ta-C is close to 0 V at neutral pH indicating that DAQ should see a positively charged surface. However, the increased number of acidic carboxylic groups on the surface provide negative charge (as they are strongly acidic) and thus will give a negative contribution to the surface charge. We do not have direct access to the resulting value, but it is possible that the net result would be slightly negative and thus would increase the adsorption strength of DAQ on ta-C surface. This is also consistent with the absence of potential shift during the backward scan as further away we are from ptzc the more positive the intrinsic surface charge would be, thus overcoming the effect of the carboxylic acid groups.
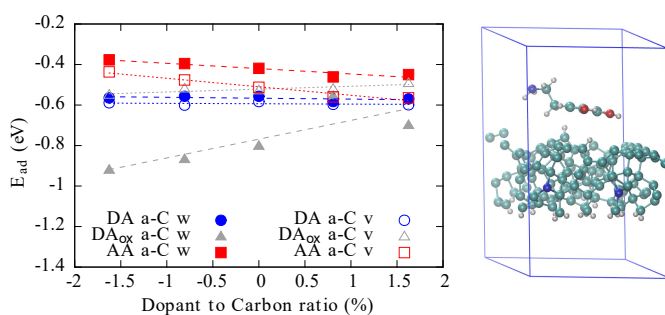

Figure 8. DA/DAQ reaction couple at formal potential. Adsorption of DAQ on the electrode surface changes its Gibbs free energy to become more negative (stabilizes it) and subsequently decreases the activation energy for the oxidation reaction inducing a cathodic shift to the oxidation peak potential.

Figure 9. On the left, adsorption energies, E_{ad}, of DA, DA$_{ox}$, and AA as a function of dopant to carbon ratio (nitrogen and boron concentrations are represented on the horizontal axis with negative and positive values, respectively) on a-C, in vacuum (v) and in dielectric medium (w). On the right an amorphous carbon system doped with two nitrogen placed at the side or in the bottom of the slab used in the calculations. The analyte, in this case DA, is placed on top of the surface (reproduced with permission from AIP [35]).

The second option is the following: as the DA oxidation to DAQ is a 2 electron + 2 proton reaction, it is possible that changes in the surface chemistry influence the tunneling of proton(s) taking place during the reaction. From the theory of proton coupled electron transfer (PCET) reactions [36] it is known that if there is a tendency for strong hydrogen bonding from the acceptor (either molecule or electrode) this tends to make the proton transfer more adiabatic and thus necessarily reduces the activation energy for tunneling. Based on the XAS results (both experimental and computational) amount of carboxylic acid groups, which are strongly hydrogen bonding, are higher in the surface of the HNO_3 treated ta-C samples. Thus, this may facilitate proton tunneling on the surface and thus result into observed cathodic shift. However, the detailed analysis of this possible mechanism is out of the scope of the present manuscript.

Conclusions

In this work we have presented an approach that can be used to understand, at least to some degree, the connections between the surface chemistry of a given material and its electrochemical performance. We showed how, by utilizing advanced computational methodologies coupled with cutting edge spectroscopy results, we can obtain atomic level information about the chemistry of the surfaces of the carbonaceous nanomaterials. Then by using these same samples for the electrochemical measurements we can draw some connections between the known atomic level surface chemistry and the observed electrochemical performance. We showed how electrical and electrostatic effects of the surface modifications can be probed by using differently charged OSR redox couples. Further, the chemical interactions can then be assessed by using the surface sensitive ISR redox couples. It is to be noted that we are still missing the computational treatment of the explicit electron and proton transfer steps in our methodology, but we are currently working on incorporating them into this approach. Thus, we argue that by using this type of approach where experimental and computational techniques are tightly integrated together, it becomes possible to gain some understanding about the physics and chemistry of

electrocatalysis. This would then enable the concept of application specific nanomaterials where surface properties are tuned for a specific application to optimize the performance of the material, by using rational data driven design.

References

[1]   Laurila T, Protopopova V, Rhode S, Sainio S, Palomäki T, Moram M, Feliu J M and Koskinen J 2014 New electrochemically improved tetrahedral amorphous carbon films for biological applications *Diam. Relat. Mater.* **49** 62–71

[2]   Medeiros R A, Matos R, Benchikh A, Saidani B, Debiemme-Chouvy C, Deslouis C, Rocha-Filho R C and Fatibello-Filho O 2013 Amorphous carbon nitride as an alternative electrode material in electroanalysis: Simultaneous determination of dopamine and ascorbic acid *Anal. Chim. Acta* **797** 30–9

[3]   Sopchak D, Miller B, Kalish R, Avyigal Y and Shi X 2002 Dopamine and Ascorbate Analysis at Hydrodynamic Electrodes of Boron Doped Diamond and Nitrogen Incorporated Tetrahedral Amorphous Carbon *Electroanalysis* **14** 473–8

[4]   Yang G, Liu E, Khun N W and Jiang S P 2009 Direct electrochemical response of glucose at nickel-doped diamond like carbon thin film electrodes *J. Electroanal. Chem.* **627** 51–7

[5]   Liu L X and Liu E 2005 Nitrogenated diamond-like carbon films for metal tracing *Surf. Coatings Technol.* **198** 189–93

[6]   Tanaka Y, Furuta M, Kuriyama K, Kuwabara R, Katsuki Y, Kondo T, Fujishima A and Honda K 2011 Electrochemical properties of N-doped hydrogenated amorphous carbon films fabricated by plasma-enhanced chemical vapor deposition methods *Electrochim. Acta* **56** 1172–81

[7]   Palomäki T, Chumillas S, Sainio S, Protopopova V, Kauppila M, Koskinen J, Climent V, Feliu J M and Laurila T 2015 Electrochemical reactions of catechol,

methylcatechol and dopamine at tetrahedral amorphous carbon (ta-C) thin film electrodes *Diam. Relat. Mater.* **59** 30–9

[8]   Yang X, Haubold L, DeVivo G and Swain G M 2012 Electroanalytical Performance of Nitrogen-Containing Tetrahedral Amorphous Carbon Thin-Film Electrodes *Anal. Chem.* **84** 6240–8

[9]   Yoo K 1999 Electrodes of Nitrogen-Incorporated Tetrahedral Amorphous Carbon A Novel Thin-Film Electrocatalytic Material with Diamond-like Stability *Electrochem. Solid-State Lett.* **2** 233

[10]   Laurila T, Sainio S and Caro M A 2017 Hybrid carbon based nanomaterials for electrochemical detection of biomolecules *Prog. Mater. Sci.* **88** 499–594

[11]   Palomäki T, Wester N, Caro M A, Sainio S, Protopopova V, Koskinen J and Laurila T 2017 Electron transport determines the electrochemical properties of tetrahedral amorphous carbon (ta-C) thin films *Electrochim. Acta* **225** 1–10

[12]   Caro M A, Deringer V L, Koskinen J, Laurila T and Csányi G 2018 Growth Mechanism and Origin of High sp3 Content in Tetrahedral Amorphous Carbon *Phys. Rev. Lett.* **120** 166101

[13]   Caro M A, Csányi G, Laurila T and Deringer V L 2020 Machine learning driven simulated deposition of carbon films: From low-density to diamondlike amorphous carbon *Phys. Rev. B* **102** 174201

[14]   Aarva A, Deringer V L, Sainio S, Laurila T and Caro M A 2019 Understanding X-ray Spectroscopy of Carbonaceous Materials by Combining Experiments, Density Functional Theory, and Machine Learning. Part I: Fingerprint Spectra *Chem. Mater.* **31** 9243–55

[15]   Aarva A, Deringer V L, Sainio S, Laurila T and Caro M A 2019 Understanding X-ray Spectroscopy of Carbonaceous Materials by Combining Experiments, Density Functional Theory, and Machine Learning. Part II: Quantitative Fitting of Spectra *Chem. Mater.* **31** 9256–67

[16]   Laurila T and Caro M A 2018 Special Features of the Electrochemistry of Undoped Tetrahedral Amorphous Carbon (ta-C) Thin Films ed K B T-E of I C Wandelt (Oxford: Elsevier) pp 856–62

[17]   Sainio S, Wester N, Aarva A, Titus C J, Nordlund D, Kauppinen E I, Leppänen E, Palomäki T, Koehne J E, Pitkänen O, Kordas K, Kim M, Lipsanen H, Mozetič M, Caro M A, Meyyappan M, Koskinen J and Laurila T 2021 Trends in Carbon, Oxygen, and Nitrogen Core in the X-ray Absorption Spectroscopy of Carbon Nanomaterials: A Guide for the Perplexed *J. Phys. Chem. C* **125** 973–88

[18]   Bartók A P, Payne M C, Kondor R and Csányi G 2010 Gaussian Approximation Potentials: The Accuracy of Quantum Mechanics, without the Electrons *Phys. Rev. Lett.* **104** 136403

[19]   Deringer V L and Csányi G 2017 Machine learning based interatomic potential for amorphous carbon *Phys. Rev. B* **95** 94203

[20]   Caro M A, Aarva A, Deringer V L, Csányi G and Laurila T 2018 Reactivity of Amorphous Carbon Surfaces: Rationalizing the Role of Structural Motifs in Functionalization Using Machine Learning *Chem. Mater.* **30** 7446–55

[21]   Deringer V L, Caro M A, Jana R, Aarva A, Elliott S R, Laurila T, Csányi G and Pastewka L 2018 Computational Surface Chemistry of Tetrahedral Amorphous Carbon by Combining Machine Learning and Density Functional Theory *Chem. Mater.* **30** 7438–45

[22]   Palomäki T, Caro M A, Wester N, Sainio S, Etula J, Johansson L-S, Han J G, Koskinen J and Laurila T 2019 Effect of Power Density on the Electrochemical Properties of Undoped Amorphous Carbon (a-C) Thin Films *Electroanalysis* **31** 746–55

[23]   Sainio S, Wester N, Titus C J, Nordlund D, Lee S, Koskinen J and Laurila T 2019 In-situ functionalization of tetrahedral amorphous carbon by filtered cathodic arc deposition *AIP Adv.* **9** 85325

[24]   Sainio S, Wester N, Titus C J, Liao Y, Zhang Q, Nordlund D, Sokaras D, Lee S, Irwin K D, Doriese W B, O'Neil G C, Swetz D S, Ullom J N, Kauppinen E I, Laurila T and Koskinen J 2019 Hybrid X-ray Spectroscopy-Based Approach To Acquire Chemical and Structural Information of Single-Walled Carbon Nanotubes with Superior Sensitivity *J. Phys. Chem. C* **123** 6114–20

[25]   Caro M A 2019 Optimizing many-body atomic descriptors for enhanced computational performance of machine learning based interatomic potentials *Phys. Rev. B* **100** 24112

[26]   Bartók A P, Kondor R and Csányi G 2013 On representing chemical environments *Phys. Rev. B* **87** 184115

[27]   De S, Bartók A P, Csányi G and Ceriotti M 2016 Comparing molecules and solids across structural and alchemical space *Phys. Chem. Chem. Phys.* **18** 13754–69

[28]   Sainio S, Nordlund D, Gandhiraman R, Jiang H, Koehne J, Koskinen J, Meyyappan M and Laurila T 2016 What Does Nitric Acid Really Do to Carbon Nanofibers? *J. Phys. Chem. C* **120** 22655–62

[29]   Clayden J, Greeves N, Warren S and Wothers P 2001 *Organic Chemistry* (Oxford University Press)

[30]   Wester N 2021 *Multilayer carbon hybrid based electrodes for direct electrochemical detection of analgesics and biomolecules - Development of an electrochemical sensor for determination of analgesics in blood samples* (Aalto University, School of Chemical Engineering)

[31]   Matsuda H and Ayabe Y 1955 Theoretical Analysis of Polarographic Waves. I. Reduction of Simple Metal Ions *Bull. Chem. Soc. Jpn.* **28** 422–8

[32]   Nicholson R S 1965 Theory and Application of Cyclic

Voltammetry for Measurement of Electrode Reaction Kinetics. *Anal. Chem.* **37** 1351–5

[33]   Wang Y, Limon-Petersen J G and Compton R G 2011 Measurement of the diffusion coefficients of [Ru(NH3)6]3+ and [Ru(NH3)6]2+ in aqueous solution using microelectrode double potential step chronoamperometry *J. Electroanal. Chem.* **652** 13–7

[34]   Weusten S J C, de Groot M T and van der Schaaf J 2020 A comparative study of the stability of hexachloroiridate and hexacyanoferrate in electrochemical mass transfer measurements *J. Electroanal. Chem.* **878** 114512

[35]   Aarva A, Laurila T and Caro M A 2017 Doping as a means to probe the potential dependence of dopamine adsorption on carbon-based surfaces: A first-principles study *J. Chem. Phys.* **146** 234704

[36]   Lam Y-C, Soudackov A V, Goldsmith Z K and Hammes-Schiffer S 2019 Theory of Proton Discharge on Metal Electrodes: Electronically Adiabatic Model *J. Phys. Chem. C* **123** 12335–45

Supporting Information
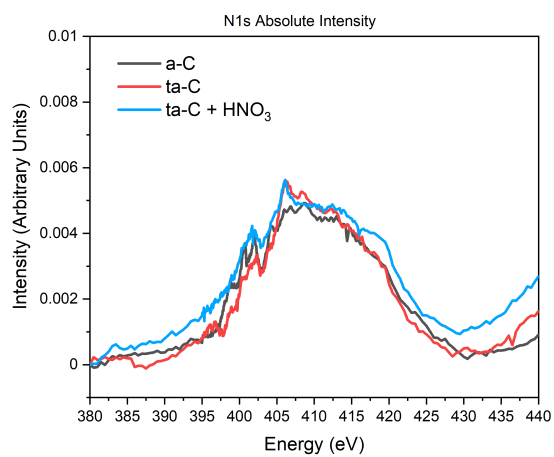
Figure S1. XAS N1s spectra from investigated carbon films.